

[CpRu((*R*)-Binop-F)(H₂O)][SbF₆], a New Fluxional Chiral Lewis Acid Catalyst: Synthesis, Dynamic NMR, Asymmetric Catalysis, and Theoretical Studies

Valérie Alezra,[†] Gérald Bernardinelli,[§] Clémence Corminboeuf,^{*,||} Urban Frey,^{*,⊥,#} E. Peter Kündig,^{*,†} André E. Merbach,[⊥] Christophe M. Saudan,[†] Florian Viton,[†] and Jacques Weber^{||}

Contribution from the Department of Organic Chemistry and Department of Physical Chemistry and Laboratory of X-ray Crystallography, University of Geneva, CH-1211 Geneva 4, Switzerland, and Institute of Chemical Sciences and Engineering, Swiss Federal Institute of Technology, CH-1015 Lausanne, Switzerland

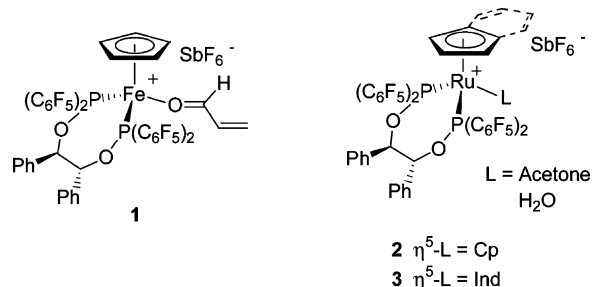
Received July 20, 2003; E-mail: peter.kundig@chiorg.unige.ch; urban.frey@hevs.ch; clemence.corminboeuf@chiphys.unige.ch

Abstract: The *C*₂-symmetric electron-poor ligand (*R*)-BINOP-F (**4**) was prepared by reaction of (*R*)-BINOL with bis(pentafluorophenyl)-phosphorus bromide in the presence of triethylamine. The iodo complex [CpRu((*R*)-BINOP-F)(I)] ((*R*)-**6**) was obtained by substitution of two carbonyl ligands by (*R*)-**4** in the in situ-prepared [CpRu(CO)₂H] complex followed by reaction with iodoform. Complex **6** was reacted with [Ag(SbF₆)] in acetone to yield [CpRu((*R*)-BINOP-F)(acetone)][SbF₆] ((*R*)-**7**). X-ray structures were obtained for both (*R*)-**6** and (*R*)-**7**. The chiral one-point binding Lewis acid [CpRu((*R*)-BINOP-F)][SbF₆] derived from either (*R*)-**7** or the corresponding aquo complex (*R*)-**8** activates methacrolein and catalyzes the Diels–Alder reaction with cyclopentadiene to give the [4 + 2] cycloadduct with an exo/endo ratio of 99:1 and an ee of 92% of the exo product. Addition occurs predominantly to the methacrolein C_α-*Re* face. In solution, water in (*R*)-**8** exchanges readily. Moreover, a second exchange process renders the diastereotopic BINOP-F phosphorus atoms equivalent. These processes were studied by the application of variable-temperature ¹H, ³¹P, and ¹⁷O NMR spectroscopy, variable-pressure ³¹P and ¹⁷O NMR spectroscopy, and, using a simpler model complex, density functional theory (DFT) calculations. The results point to a dissociative mechanism of the aquo ligand and a pendular motion of the BINOP-F ligand. NMR experiments show an energy barrier of 50.7 kJ mol⁻¹ (12.2 kcal mol⁻¹) for the inversion of the pseudo-chirality at the ruthenium center.

Introduction

Lewis acids play a key role as catalysts in organic synthesis, and applications advance at a rapid pace.¹ Our work in this area has focused on the development of stable, chiral, single point coordination transition metal Lewis acids that incorporate *C*₂-symmetric electron-poor bidentate ligands. The readily prepared, mild Fe and Ru Lewis acids **1–3** activate enals and effectively catalyze their asymmetric Diels–Alder reactions with dienes and 1,3-dipolar cycloaddition reactions with nitrones.^{2,3} The

perfluoroaryl phosphinite ligands used in **1–3** create the chiral environment around the coordination site of the enal and offset the donor properties of the cyclopentadienyl- and indenyl-ligands.



Bidentate *C*₂-symmetric chiral ligands have been widely used in asymmetric catalysis.⁴ Chiral bidentate ligands without *C*₂-

* To whom correspondence should be addressed: E.P.K. (synthesis, catalysis), U.F. (NMR), C.C. (calculations).

[†] Department of Organic Chemistry, 30 Quai Ernest Ansermet.

[§] Laboratory of X-ray Crystallography, 24 Quai Ernest Ansermet.

^{||} Department of Physical Chemistry, 30 Quai Ernest Ansermet.

[⊥] Institute of Molecular and Biological Chemistry, EPFL-BCH.

[#] Present address: University of Applied Sciences Valais (HEVs), Chemistry Department, Rte du Rawyl 64, CH-1950 Sion, Switzerland.

(1) *Handbook of Lewis Acids—Application in Organic Synthesis*; Yamamoto, H., Ed.; Wiley-VCH: Weinheim, 2000.

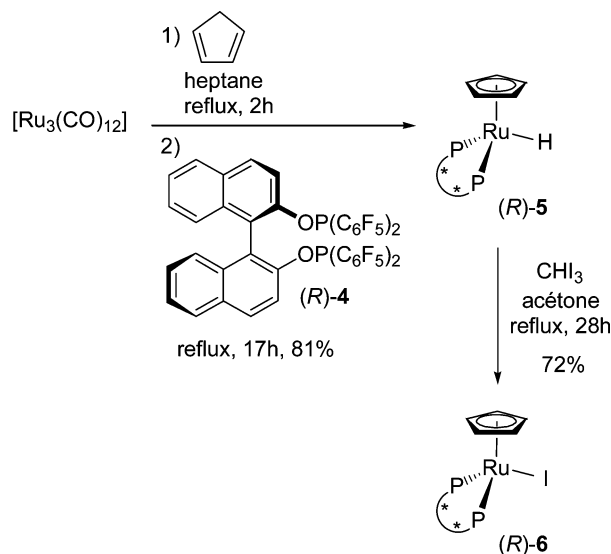
(2) (a) Kündig, E. P.; Bourdin, B.; Bernardinelli, G. *Angew. Chem., Int. Ed. Engl.* **1994**, *33*, 1856. (b) Bruin, M. E.; Kündig, E. P. *Chem. Commun.* **1998**, 2635. (c) Kündig, E. P.; Saudan, C. M.; Bernardinelli, G. *Angew. Chem., Int. Ed.* **1999**, *38*, 1220. (d) Kündig, E. P.; Saudan, C. M.; Viton, F. *Adv. Synth. Catal.* **2001**, *343*, 51. (e) Kündig, E. P.; Saudan, C. M.; Alezra, V.; Viton, F.; Bernardinelli, G. *Angew. Chem., Int. Ed.* **2001**, *40*, 4481.

(3) Viton, F.; Bernardinelli, G.; Kündig, E. P. *J. Am. Chem. Soc.* **2002**, *124*, 4968.

(4) (a) Whitesell, J. K. *Chem. Rev.* **1989**, *89*, 1581. (b) Brunner, H.; Zettlmeier, W. *Handbook of Enantioselective Catalysis*; Verlag Chemie: Weinheim, 1993; Vol. 2. (c) Noyori, R. *Asymmetric Catalysis*; John Wiley: New York, 1994.

symmetry are more recent but powerful tools for asymmetric catalysis.⁵ In CpML¹L²L³ and analogous arene complexes, the pseudotetrahedral metal is a stereogenic center. The use of chiral, dissymmetric bidentate L¹–L² ligands then leads to diastereoisomers that differ in the configuration at the metal center.^{6,7} Even when isolated, single diastereoisomers of these optically active complexes are configurationally unstable at the metal center under catalysis conditions and epimerize easily to afford mixtures of diastereomeric complexes.⁸ Some of them are nevertheless efficient catalysts for a number of asymmetric transformations because for steric and/or electronic reasons only one of the diastereoisomeric complexes is an efficient catalyst.^{7d–f} The pseudotetrahedral geometry makes this compound class particularly suitable for the study of configurational stability and configurational preference of the metal center and its role in enantioselective catalysis.⁹ The ultimate way to investigate racemization of a chiral metal center consists of the use of asymmetric complexes devoid of ligand-based chirality.^{9,10} Over the years, a number of groups have focused on applications in organic transformations of such enantiomerically pure piano-stool complexes. To the best of our knowledge, complexes with metal-based rather than ligand-based chirality have not been successfully used in asymmetric catalysis. Elegant and pioneering stoichiometric applications stem from the groups of Brunner,¹¹ Davies,¹² Faller,¹³ and Gladysz,¹⁴ among others. For asymmetric catalysis, configurational stability of the catalyst is of essence, as racemization would result in rapid erosion of enantiomeric purity of the product. Investigation of the race-

Scheme 1



mization of optically active complexes devoid of ligand-based chirality is inherently limited to chiroptical measurements.^{9c,d,10b} Computational studies have focused on the role of the ligands and the electronic configuration at the metal.¹⁵ Quantitative experimental data on the process of inversion at the metal is still scarce however.^{8,9c,d} In this article we report on a new BINOL-based Ru–Lewis acid catalyst, which catalyzes the asymmetric Diels–Alder reaction of methacrolein and cyclopentadiene.¹⁶ Its NMR characteristics suggested the complex to be suitable to probe the mechanism of the inversion of the pyramidal geometry at the metal center and establish an energy diagram for this process. The mechanistic tools used in this study include variable-temperature ¹H, ³¹P, and ¹⁷O NMR spectroscopy, variable-pressure ³¹P and ¹⁷O NMR spectroscopy,¹⁷ and, using a simpler model complex, density functional theory (DFT) calculations

Results and Discussion

Synthesis and Characterization of [CpRu((R)-BINOP-F)I] Complex. The C₂-symmetric electron-poor ligand (R)-BINOP-F **4** was prepared by reaction of (R)-BINOL with bis(pentafluorophenyl)-phosphorus bromide in the presence of triethylamine.¹⁸ The hydride complex (R)-5 was obtained by substitution of two carbonyl ligands by (R)-4 in the in situ-prepared [CpRu(CO)₂H] complex (Scheme 1).^{19,20}

- (5) For reviews, see: (a) Inoguchi, K.; Sakuraba, S.; Achiwa, K. *Synlett* **1992**, 169. (b) Frost, C. G.; Howarth, J.; Williams, J. M. J. *Tetrahedron: Asymmetry* **1992**, 3, 1089. (c) Reiser, O. *Angew. Chem., Int. Ed. Engl.* **1993**, 32, 547. For representative examples, see: (d) Jacobsen, E. N.; Zhang, W.; Güler, M. L. *J. Am. Chem. Soc.* **1991**, 113, 6703. (e) Nishiyama, H.; Yamaguchi, S.; Kondo, M.; Itoh, K. *J. Org. Chem.* **1992**, 57, 4306. (f) Rieck, H.; Helmchen, G. *Angew. Chem., Int. Ed. Engl.* **1995**, 34, 2687. (g) Schnyder, A.; Hintermann, L.; Togni, A. *Angew. Chem., Int. Ed. Engl.* **1995**, 34, 931. (h) Rajanbabu, T. V.; Casalnuovo, A. L. *J. Am. Chem. Soc.* **1996**, 118, 6325. (i) Faller, J. W.; Lloret-Fillol, J.; Parr, J. *New J. Chem.* **2002**, 26, 883.
- (6) For recent examples, see: (a) Attar, S.; Nelson, J. H.; Fischer, J.; de Cian, A.; Sutter, J.-P.; Pfeffer, M. *Organometallics* **1995**, 14, 4559. (b) Brunner, H.; Oeschey, R.; Nuber, B. *Organometallics* **1996**, 15, 3616. (c) Carmona, D.; Lahoz, F. J.; Elipse, S.; Oro, L. A.; Lamata, M. P.; Viguri, F.; Mir, C.; Cativiela, C.; Lopez-Ram de Viu, M. P. *Organometallics* **1998**, 17, 2986. (d) Carmona, D.; Vega, C.; Lahoz, F. J.; Elipse, S.; Oro, L. A.; Lamata, M. P.; Viguri, F.; Garcia-Correas, R.; Cativiela, C.; Lopez-Ramde Viu, M. P. *Organometallics* **1999**, 18, 3364. (e) Therrien, B.; Koenig, A.; Ward, T. R. *Organometallics* **1999**, 18, 1565. (f) Therrien, B.; Ward, T. R. *Angew. Chem., Int. Ed.* **1999**, 38, 405. (g) Gul, N.; Nelson, J. H. *Organometallics* **1999**, 18, 709. (h) Faller, J. W.; Parr, J. *Organometallics* **2000**, 19, 3556. (i) Drommi, D.; Faraone, F.; Francio, G.; Belletti, D.; Graiff, C.; Tiripicchio, A. *Organometallics* **2002**, 21, 761.
- (7) For recent examples, see: (a) Carmona, D.; Elipse, S.; Lahoz, F. J.; Oro, L. A.; Cativiela, C.; Pilar Lopez-Ram de Viu, M.; Pilar Lamata, M.; Vega, F.; Viguri, C. *Chem. Commun.* **1997**, 2351. (b) Davenport, A. J.; Davies, D. L.; Fawcett, J.; Garratt, S. A.; Russell, D. R. *Chem. Commun.* **1999**, 2331. (c) Davenport, A. J.; Davies, D. L.; Fawcett, J.; Garratt, S. A.; Russell, D. R. *J. Chem. Soc., Dalton Trans.* **2000**, 4432. (d) Faller, J. W.; Grimmond, B. J.; D'Allesio, D. G. *J. Am. Chem. Soc.* **2001**, 123, 2525. (e) Faller, J. W.; Parr, J. *Organometallics* **2001**, 20, 697. (f) Faller, J. W.; Grimmond, B. J. *Organometallics* **2001**, 20, 2454. (g) Faller, J. W.; Parr, J.; Lavoie, A. R. *New J. Chem.* **2003**, 27, 899.
- (8) Brunner, H.; Zwack, T. *Organometallics* **2000**, 19, 2423.
- (9) (a) Brunner, H. *Adv. Organomet. Chem.* **1980**, 18, 151. (b) Consiglio, G.; Morandini, F. *Chem. Rev.* **1987**, 87, 761. (c) Brunner, H. *Angew. Chem., Int. Ed.* **1999**, 38, 1194. (d) Brunner, H. *Eur. J. Inorg. Chem.* **2001**, 905.
- (10) (a) Brunner, H. *Angew. Chem., Int. Ed. Engl.* **1969**, 8, 38. (b) Brunner, H. *Acc. Chem. Res.* **1979**, 12, 250.
- (11) (a) Brunner, H.; Aclasis, J.; Langer, M.; Steger, W. *Angew. Chem., Int. Ed. Engl.* **1974**, 13, 810. (b) Brunner, H.; Fisch, K.; Jones, P. G.; Salbeck, J. *Angew. Chem., Int. Ed. Engl.* **1989**, 28, 1521.
- (12) (a) Davies, S. G. *Pure Appl. Chem.* **1988**, 60, 13. (b) Davies, S. G. *Aldrichim. Acta* **1990**, 23, 31.
- (13) (a) Schilling, B. E. R.; Hoffmann, R.; Faller, J. W. *J. Am. Chem. Soc.* **1979**, 101, 592. (b) Faller, J. W.; Linebarrier, D. L. *Organometallics* **1990**, 9, 3182. (c) Faller, J. W.; Ma, Y. *Organometallics* **1992**, 11, 2726.

- (14) (a) Dalton, D. M.; Fernandez, J. M.; Emerson, K.; Larsen, R. D.; Arif, A. M.; Gladysz, J. A. *J. Am. Chem. Soc.* **1990**, 112, 9198. (b) Dalton, D. M.; Garner, C. M.; Fernandez, J. M.; Gladysz, J. A. *J. Org. Chem.* **1991**, 56, 6823. (c) Klein, D. P.; Gladysz, J. A. *J. Am. Chem. Soc.* **1992**, 114, 8710. (d) Gladysz, J. A.; Boone, B. J. *Angew. Chem., Int. Ed. Engl.* **1997**, 36, 550.
- (15) (a) Ward, T. R.; Schafer, O.; Daul, C.; Hofmann, P. *Organometallics* **1997**, 16, 3207. (b) Costuas, K.; Saillard, J.-Y. *Organometallics* **1999**, 18, 2505. (c) Smith, K. M.; Poli, R.; Legzdins, P. *Chem. Commun.* **1998**, 1903. (d) Yang, Y.; Asplund, M. C.; Kotz, K. T.; Wilkens, M. J.; Frei, H.; Harris, C. B. *J. Am. Chem. Soc.* **1998**, 120, 10154.
- (16) (a) Kagan, H. B.; Riant, O. *Chem. Rev.* **1992**, 92, 1007. (b) Pindur, U.; Lutz, G.; Otto, C. *Chem. Rev.* **1993**, 93, 741. (c) Oh, T.; Reilly, M. *Org. Prep. Proced. Int.* **1994**, 26, 129. (d) Dias, L. C. *J. Braz. Chem. Soc.* **1997**, 8, 289. (e) Corey, E. J.; Guzman-Perez, A. *Angew. Chem., Int. Ed.* **1998**, 37, 389. (f) Soudan, C.; Kündig, E. P. In *Handbook of Lewis Acids*; Yamamoto, H., Ed.; VCH-Wiley: Weinheim, 2000; pp 597–652. (g) Nicolaou, K. C.; Snyder, S. A.; Montagnon, T.; Vassilikogiannakis, G. *Angew. Chem., Int. Ed.* **2002**, 41, 1668. (h) Corey, E. J. *Angew. Chem., Int. Ed.* **2002**, 41, 1650.
- (17) Helm, L.; Merbach, A. E. *J. Chem. Soc., Dalton Trans.* **2002**, 633.

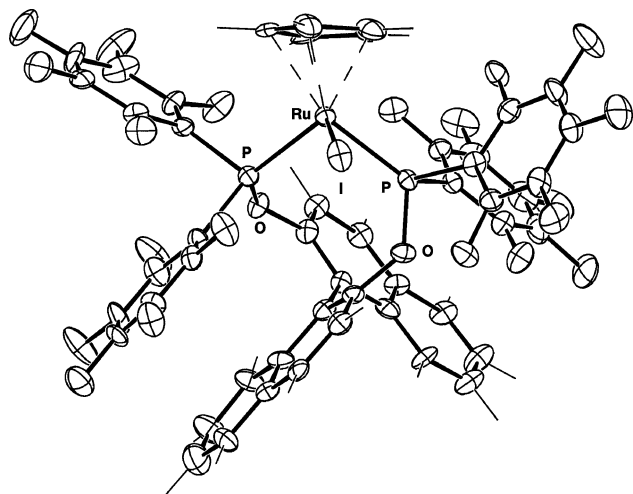


Figure 1. ORTEP view of the crystal structure of [CpRu((R)-BINOP-F)](R)-6 with 40% probability ellipsoids. Selected bond lengths (Å) and bond angles (deg): Ru–P = 2.298(3), 2.271(4); Ru–I = 2.735(1); Cp_(mean plane)••Ru = 1.851(1); P–Ru–P = 99.0(1); I–Ru–P = 84.0(1), 107.2(1).

The hydride-labilizing effect was crucial to the success of CO substitution.²¹ Attempts to carry out this ligand exchange in the analogous chloro complex were not successful. The robust air-stable hydrido complex (R)-5 was isolated from the crude mixture by column chromatography (aluminum oxide, neutral). Its ¹H NMR spectrum in CD₂Cl₂ showed a doublet of doublets at δ = –11.82 ppm for the Ru–H proton.²² Subsequent treatment with iodoform in refluxing acetone afforded the air-stable iodo complex (R)-6.²³ Crystals suitable for X-ray diffraction analysis were obtained from a CH₂Cl₂/MeOH solution (Figure 1).

Synthesis, Characterization, and Catalytic Behavior of [CpRu((R)-BINOP-F)L][SbF₆] (L = Acetone, H₂O) Complexes. Reaction of a red-orange solution of (R)-6 in acetone/CH₂Cl₂ with AgSbF₆ generated the yellow cationic complex (R)-7, which was isolated by precipitation with Et₂O after concentration of the acetone/CH₂Cl₂ mixture (Scheme 2).

Crystals suitable for X-ray diffraction analysis were obtained by slow diffusion of Et₂O into a solution of (R)-7 in acetone (Figure 2).

The Diels–Alder reaction of methacrolein and cyclopentadiene (1 mol % catalyst, CH₂Cl₂, –20 °C) was used as a test reaction. Reaction occurred at a similar rate as that of the previously reported complexes [CpRu(BIPHOP-F)L][SbF₆] (L = acetone, H₂O) 2.^{2c,d} The cycloadduct 9 was isolated in 92% yield, with a *exo:endo* diastereomeric ratio of 99:1, an enantioselectivity of 92% ee (*exo*) and 2*S* absolute configuration (Scheme 3). The aquo complex (R)-8 was formed upon addition

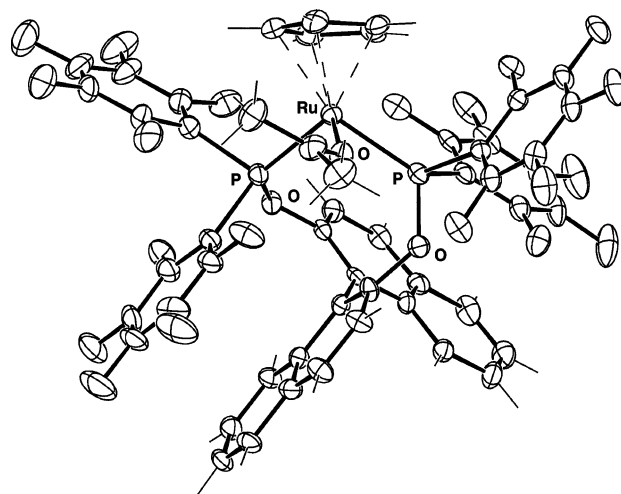
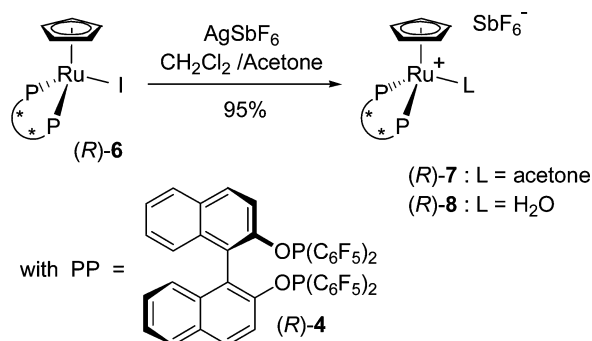
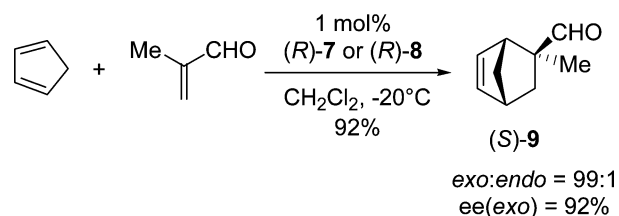


Figure 2. ORTEP view of the crystal structure of [CpRu((R)-BINOP-F)(acetone)][SbF₆] (R)-7 with 30% probability ellipsoids. Selected bond lengths (Å) and bond angles (deg): Ru–P = 2.306(3), 2.297(3); Ru–O = 2.162(8); Cp_(mean plane)•••Ru = 1.872(1); P–Ru–P = 100.3(1); O–Ru–P = 81.2(2), 105.0(2).

Scheme 2



Scheme 3



of water to a solution of (R)-7 in acetone.²⁴ The aquo ligand is labile, and this provides another entry to the active catalytic species, the results obtained in the test Diels–Alder reaction being identical in terms of activity and selectivity to those obtained with the acetone complex (R)-7. Ligand 4 forms a nine-membered metallacycle upon coordination to Ru, whereas BIPHOP-F (e.g., in complex 2) forms a seven-membered metallacycle. The effect on the shape of the chiral site of the catalyst is minor though, and it looks very similar to that of 2. The enantioselectivity and the sense of asymmetric induction are identical in both cases.

Upon complexation to the metal, the C₂-symmetry of the free ligand (R)-4 is lost. Indeed, in the pseudotetrahedral complexes

(18) Kündig, E. P.; Dupré, C.; Bourdin, B.; Cunningham, Jr., A. F.; Pons, D. *Helv. Chim. Acta* **1994**, *77*, 421.

(19) For a listing of synthetic routes to [CpRuLL'X] complexes, see: Shen, J.; Stevens, E. D.; Nolan, S. P. *Organometallics* **1998**, *17*, 3000.

(20) Bruce, M. I.; Jensen, C. M.; Jones, N. L. *Inorg. Synth.* **1990**, *28*, 216.

(21) Baldoivino, C.; Cesarotti, E.; Prati, L. *Gazz. Chim. Ital.* **1992**, *122*, 475 and references therein.

(22) (η^5 -Arene)RuHL₂ complexes: (a) Deeming, A. J.; Speel, D. M.; Stchedroff, M. *Organometallics* **1997**, *16*, 6004. (b) Wiles, J. A.; Bergens, S. H. *Organometallics* **1998**, *17*, 2228. (c) Geldbach, T. J.; Pregosin, P. *Helv. Chim. Acta* **2002**, *85*, 3937. (d) Geldbach, T. J.; Pregosin, P.; Albinati, A. *J. Chem. Soc., Dalton Trans.* **2002**, 2419.

(23) Bruce, M. I.; Humphrey, M. G.; Swincer, A. G.; Wallis, R. C. *Aust. J. Chem.* **1984**, *37*, 1747.

(24) Aquo complexes of organometallic Lewis acids are frequently observed. Some examples are given in refs 6c,d,f and 7a–c,e,f and in the following: (a) Takahashi, Y.; Akita, M.; Hikichi, S.; Morooka, Y. *Inorg. Chem.* **1998**, *37*, 3186. (b) Takahashi, Y.; Hikichi, S.; Akita, M.; Morooka, Y. *Chem. Commun.* **1999**, 1491.

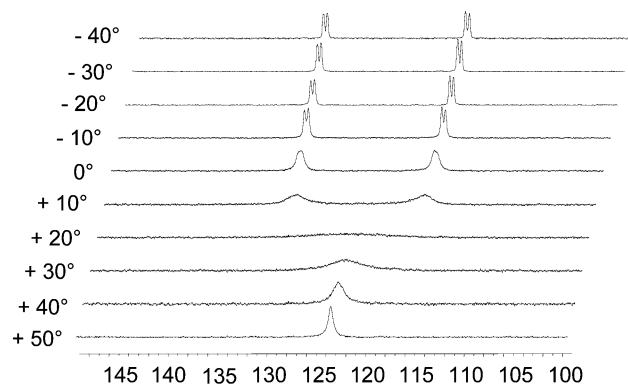


Figure 3. Variable-temperature ^{31}P NMR stack plot of $[\text{CpRu}((R)\text{-BINOP-F})(\text{H}_2\text{O})][\text{SbF}_6]$ ($(R)\text{-8}$) ($[(R)\text{-7}] = 0.05 \text{ mol L}^{-1}$, $[\text{H}_2\text{O}] = 1.20 \text{ mol L}^{-1}$, acetone- d_6).

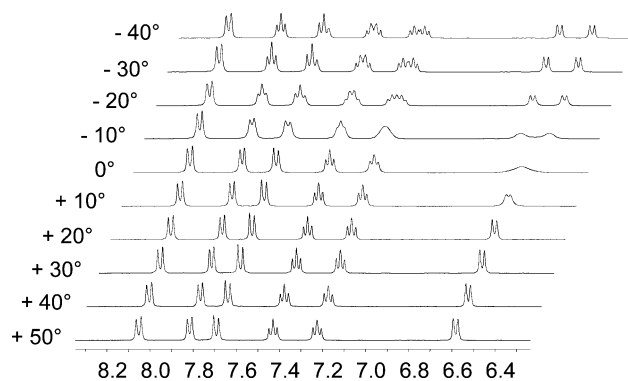


Figure 4. Variable-temperature ^1H NMR stack plot of $[\text{CpRu}((R)\text{-BINOP-F})(\text{H}_2\text{O})][\text{SbF}_6]$ ($(R)\text{-8}$) ($[(R)\text{-7}] = 0.05 \text{ mol L}^{-1}$, $[\text{H}_2\text{O}] = 1.20 \text{ mol L}^{-1}$, acetone- d_6).

$[\text{CpRu}(\text{PP})\text{X}]$, where PP is a C_2 -symmetric bidentate ligand, the two diastereotopic phosphorus give a characteristic AB quartet. This AB pattern is actually observed in ^{31}P NMR (acetone- d_6) of the hydrido and iodo complexes ($(R)\text{-5}$ and ($(R)\text{-6}$). In contrast, the ^{31}P NMR spectra (acetone- d_6) of the cationic complexes ($(R)\text{-7}$ and ($(R)\text{-8}$) at room temperature show a singlet for the two diastereotopic P nuclei of the bidentate ligand. The presence of a singlet resulting from coincidental signal overlap was excluded by the observation of the usual AB quartet at -40°C for ($(R)\text{-7}$) and ($(R)\text{-8}$) (Figure 3). The previously reported indenyl complexes **3** showed similar ^{31}P NMR behavior,^{2c} very different from the cyclopentadienyl analogues **2**, which gave an AB quartet (acetone- d_6 , room temperature).^{2c}

^1H and ^{13}C NMR spectra of complexes ($(R)\text{-7}$) and ($(R)\text{-8}$) in acetone- d_6 at room temperature showed a simple system of signals for the coordinated ($(R)\text{-BINOP-F}$) ligand (10 carbon signals and 6 proton signals for the binaphthyl backbone), similar to those observed for the noncoordinated ($(R)\text{-BINOP-F}$) (**4**). In comparison, complexes ($(R)\text{-5}$) and ($(R)\text{-6}$), as expected, display different signals for all 20 carbons and 12 protons of the binaphthyl backbone. On cooling ($(R)\text{-8}$) to -40°C , the resonances assigned to the ($(R)\text{-BINOP-F}$) ligand split into two sets and became sharper (Figure 4). In addition, the ^1H NMR spectrum of the aquo complex ($(R)\text{-8}$) in acetone- d_6 at -40°C showed two singlets at 5.50 and 3.91 ppm for the coordinated and free water, respectively. At room temperature, a single, averaged signal at 3.18 ppm is apparent.

The above observations point to a fluxional process that renders the P atoms equivalent and results in a rapid exchange

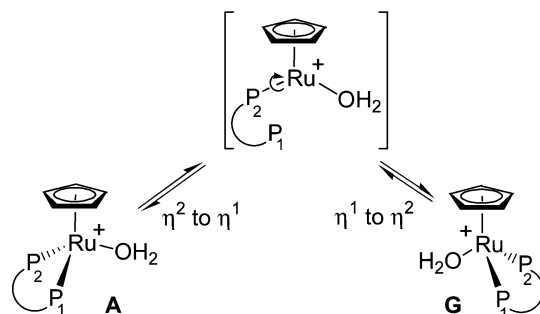


Figure 5. Inversion of ($(R)\text{-8}$) via a $\eta^2\text{-}\eta^1\text{-}\eta^2$ hemidissociation mechanism

between two identical structures of the complexes and an inversion at the chirotopic metal center.²⁵ Literature precedent includes the indenyl ruthenium complex **3**^{2c} and arene ruthenium²⁶ and Cp* rhodium²⁷ complexes bearing C_2 -symmetric bisoxazoline ligands. For more detailed mechanistic investigation we chose the aquo complex ($(R)\text{-8}$) rather than the acetone complex ($(R)\text{-7}$), which was always contaminated by small amounts of **8** due to the presence of residual traces of water.

Mechanism. The temperature-dependence of the NMR spectra of ($(R)\text{-8}$) is attributed to the interconversion of the two identical structures **A** and **G** (Figures 5 to 8). If we limit the analysis to processes that involve either 18- or 16-electron intermediates, a first possible mechanism for this inversion at the chirotopic metal center is dissociation/recoordination of one of the P termini of the chiral chelating ligand as shown in Figure 5.

Alternatively, and much more likely in view of the behavior of **8** in catalysis, interconversion may take place via a sequence that involves dissociation of the water molecule, inversion of the nine-membered metallacycle in $[\text{CpRu}((R)\text{-BINOP-F})]^+$, and reassociation of the H_2O ligand. In turn, this process may occur either via a dissociative D mechanism (Figure 6) or a dissociative interchange I_d (Figure 7). In addition, this swing motion may also proceed through an associative H_2O exchange with inversion at ruthenium and haptotropic $\eta^5 \rightleftharpoons \eta^3$ rearrangement of the Cp ligand (Figure 8).

An analysis of the mechanistic schemes in Figures 6–8 was carried out by a combination of variable-temperature and -pressure ^{31}P and ^{17}O NMR experiments and DFT calculations.

Mechanism Attribution. (a) ^{17}O NMR; Water Exchange. The ^{17}O NMR spectra of a solution of 0.05 mol L^{-1} ($(R)\text{-8}$) and 0.5 mol L^{-1} 38% ^{17}O enriched H_2O in acetone- d_6 at 273 K shows a signal at 0 ppm for the free water (reference) and a small and broad signal at -160 ppm corresponding to the coordinated water molecule. The water exchange on ($(R)\text{-8}$) in acetone (eq 1) was followed by ^{17}O NMR spectroscopy, and a line shape analysis of the resulting NMR spectra afforded the detailed kinetic parameters. The derived kinetic parameters for the variable-temperature and -pressure studies of water exchange on ($(R)\text{-8}$) are shown in Table 1. The water exchange rate constant (k_{ex}) observed in acetone solutions ($[(R)\text{-8}] = 0.025 \text{ mol L}^{-1}$)

- (25) (a) Mislow, K. *J. Am. Chem. Soc.* **1984**, *106*, 3319. (b) Eliel, E. L.; Wilen, S.; Mander, L. N. *Stereochemistry of Organic Compounds*; Wiley & Sons: New York, 1994; pp 53 and 1195.
 (26) (a) Asano, H.; Katayama, K.; Kurosawa, H. *Inorg. Chem.* **1996**, *35*, 5760. (b) Kurosawa, H.; Asano, H.; Miyaki, Y. *Inorg. Chim. Acta* **1998**, *270*, 87. (c) Faller, J. W.; Lavoie, A. *J. Organomet. Chem.* **2001**, *630*, 17. (d) Davies, D. L.; Fawcett, J.; Garratt, S. A.; Russell, D. R. *Organometallics* **2001**, *20*, 3029.
 (27) Davies, D. L.; Fawcett, J.; Garratt, S. A.; Russell, D. R. *J. Organomet. Chem.* **2002**, *662*, 43.

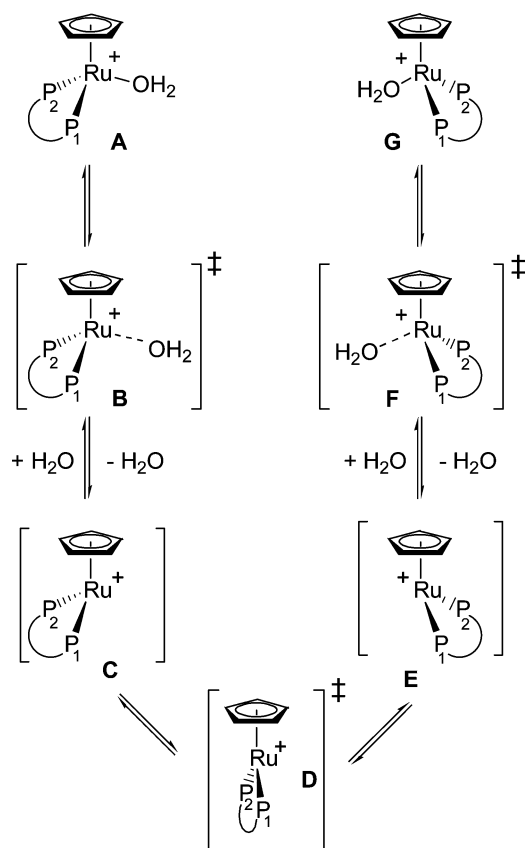


Figure 6. Inversion of (R)-8 via a two-step dissociative *D* mechanism.

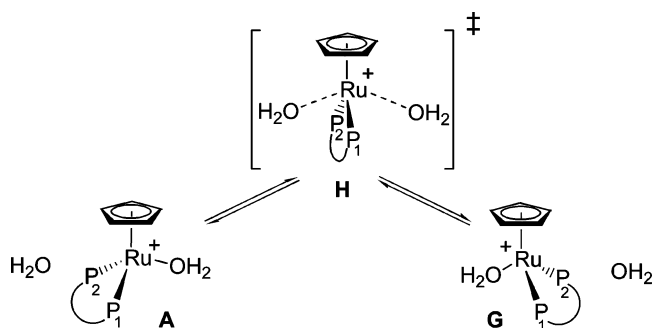


Figure 7. Inversion of (R)-8 via a dissociative interchange *I_a* mechanism.

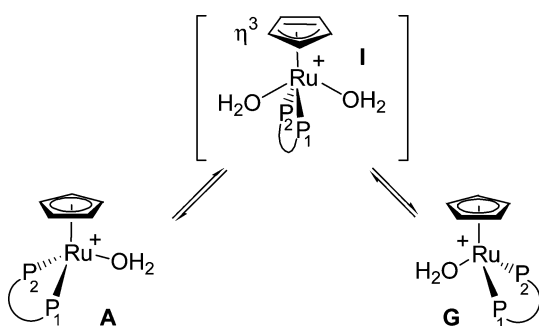


Figure 8. Inversion of (R)-8 via an associative mechanism with haptotropic $\eta^5 \rightleftharpoons \eta^3$ rearrangement of the Cp ligand.

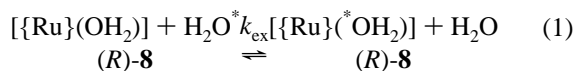
showed no water concentration dependence ($[\text{H}_2\text{O}] = 0.56\text{--}2.25 \text{ mol L}^{-1}$) at 291 K (see Supporting Information). Also, no dependence with added HSbF_6 was observed (see Supporting Information). The positive volume of activation, as well as the first-order rate constant, first order in complex concentration and zero order in water concentration, are in accordance with a

Table 1. Derived Kinetic Parameters for the Variable-Temperature and -Pressure Studies of Water Exchange and Swing Motion on (R)-8 in Acetone

	water exchange	swing motion
k_{ex}^{298a} (s ⁻¹)	29 200 ± 400	8370 ± 630
ΔH^\ddagger (kJ mol ⁻¹)	50.57 ± 1.4	79.14 ± 1.8
ΔS^\ddagger (J mol ⁻¹ K ⁻¹)	10.15 ± 4.9	95.60 ± 6.5
$\Delta V^{\ddagger b}$ (cm ³ mol ⁻¹)	4.8 ± 0.6	11.6 ± 0.3
$\Delta G^{\ddagger 298}$ (kJ mol ⁻¹)	47.54 ± 0.03	50.65 ± 0.40

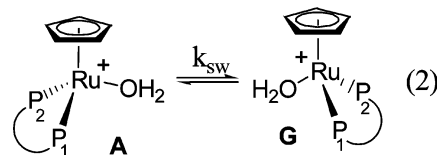
^a k_{ex} (water exchange); k_{sw} (swing motion). ^b At 293.4 K.

dissociative mode of activation, and the modest value of ΔV^\ddagger does support an *I_a* mechanism for the water molecule exchange.



Parameters for water and acetonitrile exchange on a number of ruthenium(II) complexes are given in Table 2. Both H₂O and MeCN are greatly labilized by nonleaving π -bonding ligands. The kinetic trans effect increases the lability by 6×10^{10} -fold along the sequence $[\text{Ru}(\text{MeCN})_6]^{2+} < [\text{Ru}(\eta^6\text{-C}_6\text{H}_6)(\text{MeCN})_3]^{2+} < [\text{Ru}(\eta^5\text{-C}_5\text{H}_5)(\text{MeCN})_3]^+$ (Table 2, entries 1–3) and is a consequence of a corresponding decrease in ΔH^\ddagger . It is also accompanied by an increasingly strong d-activation mode as indicated by the growing ΔV^\ddagger . A similar trend is also observed for the aquo complexes (Table 2, entries 4–6). We therefore can explain the high rate constant, as well as the strengthened d-activation mode on (R)-8, by the strong labilizing effect of the $\eta^5\text{-C}_5\text{H}_5$ ligand (Table 2, entries 3 and 6).

(b) ³¹P NMR; Inversion at Ru. The kinetic parameters for the swing motion (eq 2, Figures 5–8) were determined using variable-temperature and variable-pressure ³¹P NMR spectroscopy.



Detailed kinetic parameters of the ³¹P NMR study are shown in Table 1. No dependence of the swing motion rate constant (k_{sw}) with respect to added HSbF_6 was observed. The positive volume and entropy of activation are in accordance with a dissociative mode of activation (*I_a* or *D* mechanisms). Considering the high ΔV^\ddagger value along with a positive ΔS^\ddagger value, it is tempting to assign this to a $\eta^2\text{-}\eta^1\text{-}\eta^2$ hemidissociation process of the (R)-BINOP-F ligand. However, neither synthetic properties nor NMR measurements substantiate this interpretation. From the observation of different inversion barriers in three Cp*Rh(bisoxazoline) complexes, Davies et al. also concluded that hemidissociation of one oxazoline moiety was an unlikely process.²⁷ While we cannot completely exclude this possibility, a more likely event is the dissociation of water that triggers the movement of inversion. In addition, failure to observe similar fluxional behaviors in the hydrido and iodo analogues (R)-5 and (R)-6 support this interpretation.^{26,31}

(28) Rapaport, I.; Helm, L.; Merbach, A. E.; Bernhard, P.; Ludi, A. *Inorg. Chem.* **1988**, *27*, 873.

(29) Luginbühl, W.; Zbinden, P.; Pittet, P.-A.; Armbruster, T.; Bürgi, H.-B.; Merbach, A. E.; Ludi, A. *Inorg. Chem.* **1991**, *30*, 2350.

Table 2. Parameters for Solvent Exchange on Ruthenium(II) Complexes

entry	complex	k_{ex}^{298} (s ⁻¹) ^a	ΔH^\ddagger (kJ mol ⁻¹)	ΔS^\ddagger (J mol ⁻¹ K ⁻¹)	ΔV^\ddagger (cm ³ mol ⁻¹)	ref
1	[Ru(CH ₃ CN) ₆] ²⁺	8.9×10^{-11}	140.3	33.3	0.4	28
2	[Ru(η^6 -C ₆ H ₆)(CH ₃ CN) ₃] ²⁺	4.1×10^{-5}	102.5	15.0	2.4	29
3	[Ru(η^5 -C ₅ H ₅)(CH ₃ CN) ₃] ⁺	5.6	86.5	59.6	11.1	29
4	[Ru(H ₂ O) ₆] ²⁺	1.8×10^{-2}	87.8	16.1	-0.4	28
5	[Ru(η^6 -C ₆ H ₆)(H ₂ O) ₃] ²⁺	11.5	75.9	29.9	1.5	30
6	(<i>R</i>)- 8	2.9×10^4	50.6	10.2	4.8	this study

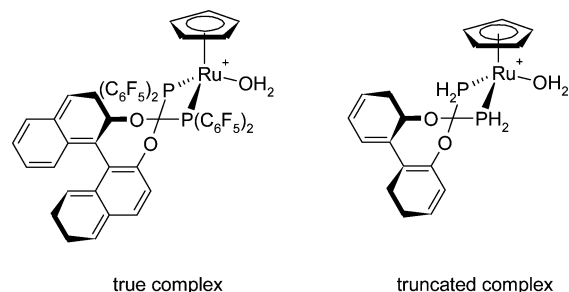
^a Rate constant for the exchange of a particular coordinated solvent molecule.

As shown in Table 1, the rate constant of the water exchange process k_{ex} is about three times higher than the one of the (*R*)-BINOP-F swing motion, k_{sw} . This may reflect the two different possibilities of a water molecule to be exchanged in a dissociative mechanism. Indeed, the entering water molecule may exchange either from the same side or from the opposite side of the outgoing ligand, only the second possibility implying a swing motion of the bidentate ligand. To complete experimental observations and provide further information on the exact dissociative process, *D* and *I_d* mechanisms were subjected to computational analysis. Note that the associative mechanisms have not been considered in our calculations, since the activation parameters obtained previously do not support such a mechanism. Moreover, it has been shown previously that the approach of an additional ligand to a coordinatively saturated Ru(II) complex is electrostatically disfavored.³²

(c) Calculations. Geometry optimization and electronic structure calculations were performed with the Gaussian98 and Gaussian03 programs.³³ The DZVP³⁴ basis set were employed with density functional theory using the PW91 functional.³⁵

To reduce computation time, most of the calculations were performed on a truncated complex, in which the ligand BINOP-F was replaced by H₂PO(C₆H₄)₂OPH₂.

While this simplification appears severe, it is expected to provide helpful insight into the mechanism operative in other [CpRu(PP)L]⁺-based compounds such as (*R*)-**8**. Of course, when considering the energy barrier, we will have to keep in mind the electronic effect caused by the π -acid BINOP-F ligand. As a further approximation, the counterion as well as the explicit quantum-mechanical treatment of solvent were neglected, as it would have been too time-consuming with today's computational possibilities.³⁶ However, quantum mechanics and mo-



lecular mechanics (QM/MM) approaches seem to be well suited for performing explicit solvation simulations.^{37,38} For the calculation of solvent exchange or racemization processes, the solvent is frequently neglected^{39–42} or treated implicitly using a continuum model.^{43,44} In this study, solvent effects were taken into account statically by means of polarized continuum model (PCM) calculations⁴⁵ using a self-consistent field technique as implemented in Gaussian03.^{33b,45d} In this model a quantum mechanically treated solute molecule is placed within the so-called solute cavity. The shape and dimensions of the cavity are determined by the molecular structure. The cavity is surrounded by a continuum dielectric polarized by the solute molecule. In turn, the dielectric polarization generates an electrostatic field at the solute molecule, modifying its electron density. Free energies of solvation were calculated with acetone as a solvent following the experimental conditions ($\epsilon = 20.7$). The geometries were kept optimized as for the gas-phase species (single-point calculations). Due to the rigidity of the structures involved, optimization within PCM changes the relative energies and bond lengths by less than 0.5 kcal mol⁻¹ and 0.5 Å, respectively, as it was tested for two geometries (see Table S-11 and S-13 in Supporting Information).

Minimum energy optimizations of the gas-phase structures were based on complete geometry optimizations. Transition state calculations were obtained following the correct normal mode manually or using the transition-state optimization type as implemented in the Gaussian98 program.^{33a} Frequency calcula-

- (30) Stebler-Röthlisberger, M.; Hummel, W.; Pittet, P.-A.; Bürgi, H.-B.; Ludi, A.; Merbach, A. E. *Inorg. Chem.* **1988**, *27*, 1358.
- (31) For related discussions, see for example: (a) Slugovc, C.; Simanko, W.; Mereiter, K.; Schmid, R.; Kirchner, K.; Xiao, L.; Weissensteiner, W. *Organometallics* **1999**, *18*, 3865. (b) Faller, J. W.; Grimmond, B. J.; Curtis, M. *Organometallics* **2000**, *19*, 5174.
- (32) De Vito, D.; Sidorenkova, H.; Rotzinger, F. P.; Weber, J.; Merbach, A. E.; *Inorg. Chem.* **2000**, *39*, 5547.
- (33) (a) Frisch, M. J.; Trucks, G. W.; Schlegel, H. B.; Scuseria, G. E.; Robb, M. A.; Cheeseman, J. R.; Zakrzewski, V. G.; Montgomery, J. A., Jr.; Stratmann, R. E.; Burant, J. C.; Dapprich, S.; Millam, J. M.; Daniels, A. D.; Kudin, K. N.; Strain, M. C.; Farkas, O.; Tomasi, J.; Barone, V.; Cossi, M.; Cammi, R.; Mennucci, B.; Pomelli, C.; Adamo, C.; Clifford, S.; Ochterski, J.; Petersson, G. A.; Ayala, P. Y.; Cui, Q.; Morokuma, K.; Malick, D. K.; Rabuck, A. D.; Raghavachari, K.; Foresman, J. B.; Cioslowski, J.; Ortiz, J. V.; Stefanov, B. B.; Liu, G.; Liashenko, A.; Piskorz, P.; Komaromi, I.; Gomperts, R.; Martin, R. L.; Fox, D. J.; Keith, T.; Al-Laham, M. A.; Peng, C. Y.; Nanayakkara, A.; Gonzalez, C.; Challacombe, M.; Gill, P. M. W.; Johnson, B. G.; Chen, W.; Wong, M. W.; Andres, J. L.; Head-Gordon, M.; Replogle, E. S.; Pople, J. A. *Gaussian 98*, revision A.8; Gaussian, Inc.: Pittsburgh, PA, 1998. (b) Gaussian 03, revision A.1; Gaussian, Inc., Pittsburgh, PA, 2003.
- (34) Godbout, N.; Salahub, D. R.; Andzelm, J.; Wimmer, E. *Can. J. Chem.* **1992**, *70*, 560.
- (35) Perdew, Wang, Y. *Electronic Structure of Solids '91*; 1991; p 11.
- (36) Erras-Hanauer, H.; Clark, T.; van Eldik, R. *Coord. Chem. Rev.* **2003**, *238*, 233.

- (37) (a) Gao, J. In *Reviews in Computational Chemistry*; Lipkowitz, K. B., Boyd, D. B., Eds.; VCH: New York, 1996; Vol. 7. (b) Gao, J.; Xia, X. *Science* **1992**, *258*, 631. (c) Gao, J.; Xia, X. *J. Phys. Chem.* **1992**, *96*, 537.
- (38) Woo, T. K.; Blöchl, P. E.; Ziegler, T. *J. Mol. Struct. (THEOCHEM)* **2000**, *506*, 313.
- (39) Rotzinger, F. P. *J. Am. Chem. Soc.* **1996**, *118*, 6760.
- (40) Kowall, Th.; Caravan, P.; Bourgeois, H.; Helm, L.; Rotzinger, F. P.; Merbach, A. E. *J. Am. Chem. Soc.* **1998**, *120*, 6569.
- (41) Hartmann, M.; Clark, T.; van Eldik, R. *J. Phys. Chem. A* **1999**, *103*, 9899.
- (42) Robitzer, M.; Ritzel, V.; Sirlin, C.; Dedieu, A.; Pfeffer, M. C. R. *Chimie* **2002**, *5*, 467.
- (43) Cramer, C. J.; Truhlar, D. G. In *Reviews in Computational Chemistry*; Lipkowitz, K. B., Boyd, D. B., Eds.; VCH: New York, 1995; Vol. 6.
- (44) Tomasi, J. *Chem. Rev.* **1994**, *94*, 2027.
- (45) (a) Miertus, S.; Tomasi, J. *Chem. Phys.* **1982**, *65*, 239. (b) Miertus, S.; Scrocco, E.; Tomasi, J. *J. Chem. Phys.* **1981**, *55*, 117. (c) Mennucci, B.; Cancès, E.; Tomasi, J. *J. Phys. Chem. B* **1997**, *101*, 10506. (d) Cossi, M.; Scalmani, G.; Rega, N.; Barone, V. *J. Chem. Phys.* **2002**, *117*, 43. (e) Scalmani, G.; Barone, V.; Kudin, K. N.; Pomelli, C. S.; Scuseria, G. E.; Frisch, M. J. *Theo. Chem. Acc.* **2003**, submitted.

Table 3. Geometrical Parameters of (R)-**8** at the PW91/3-21G* Level and Truncated **A–D** and **H** at the PW91/DZVP Level Compared to the X-ray Structure of (R)-**7**

	truncated PW91/DZVP					entire PW91/3-21G*	
	A	B	C	D	H	(R)- 8	(R)- 7 X-ray
R(Ru–P) Å	2.30	2.33	2.32	2.37	2.36	2.28	2.30
R(P–O) Å	1.69	1.70	1.68	1.67	1.68	1.66	1.61
R(C _p centroid–Ru) Å	1.88	1.85	1.85	1.82	1.81	1.92	1.87
R(Ru–L) Å	2.28	3.25			3.81/3.85	2.18	2.16
θ(P–Ru–P)	99.2	99.3	99.9	102.6	107.2	102.1	100.3
θ(P–Ru–C _p centroid)	122.4	123.5	124.8	128.7	126.3	121.0	123.5
θ(H–P–H) or θ(C–P–C)	98.4	98.7	99.0	98.8	99.2	98.8	98.7
θ(H–P–O) or θ(C–P–O)	98.5	98.9	99.8	100.1	99.7	97.6	97.0
φ (C _p centroid–Ru–P–P)	–138.5	–141.2	–144.2	–179.0	–175.0	–137.9	–136.6
φ (H–P–H–O)	96.7	96.5	98.1	98.5	99.9	97.1	98.8
or φ (C–P–C–O)							

Table 4. Energies, Enthalpies, and Free Energies in the Gas Phase for the Racemization of **A** at the PW91/DZVP Level and PCM Estimates of the Free Energy of Solvation in Acetone^{a,b}

	<i>D</i>			<i>I_d</i>
	ΔA–B	ΔA–(C + H ₂ O)	ΔA–(D + H ₂ O)	Δ(A + H ₂ O)–H
gas phase				
Δ(<i>E</i> + ZPE)	+58.26	+107.79	+110.00	+52.07
Δ <i>H</i> ^{gas} (298.15 K)	+57.59	+102.27	+114.05	+55.41
Δ <i>G</i> ^{gas} (298.15 K)	+57.09	+52.07	+66.80	+68.57
liquid phase ε = 20.7				
ΔΔ <i>G</i> _{solv}	+7.61	–14.10	–11.09	+16.26
<i>RT</i> ln(1/22.4)	–7.71	–7.71	–7.71	–7.71
Δ <i>G</i> ^{sol} (298.15 K)	+56.99	+30.26	+48.00	+77.12

^a At 298.15 K. All energies are in kJ mol^{–1}. Δ*H*^{gas} and Δ*G*^{gas} are values from gas-phase calculations with Δ*H*^{gas} = Δ(*H*_{trans} + *H*_{rot} + *H*_{vib} + *H*_{ZPE} + *E*_{elec}) and Δ*G*^{gas} = Δ*H*^{gas} – *T*Δ*S*^{gas}. (see ref 46 for more details). Δ*G*^{sol} = Δ*G*^{gas} + ΔΔ*G*_{solv} + *RT*ln(1/22.4), note that “reduced” solvation energy is used, in which the difference between the molecular motion contributions calculated in vacuo and in solution is neglected. ΔΔ*G*_{solv} is given by the PCM calculation.

^b Vibrational entropy does not include any low-frequency modes corresponding to internal rotation.^{46,54}

tions were performed for all minima and transition states in the gas phase. Each transition state was characterized by a single imaginary vibrational frequency, whereas reactants and products had no imaginary frequency. Moreover, frequency calculations were also performed to provide an estimate of the thermal correction to the activation enthalpy and entropy within the standard harmonics oscillator/rigid rotator/ideal gas approximation.^{46,47} The calculation of vibrational frequencies, already very demanding for the isolated complex, is even more tedious within the PCM approach and has not been achieved. Therefore, for the thermochemical corrections of the liquid phase, the gas-phase data were taken as the first approximation, but it is common practice to neglect the changes in thermal motion and to use a “reduced” solvation free energy.^{45c,48} A listing of Cartesian coordinates and total energies of all the reactants, intermediates, and transition states can be found in Supporting Information (see Table S-11–16).

Geometrical Parameters. Previous benchmark calculations of **A** have been performed on the full structure with the smaller 3-21G* basis set to enable a comparison of the most relevant geometrical parameters, in particular those located in the vicinity of the coordinated sites. Some of the most significant geometrical parameters were compared with the X-ray structure of (R)-**7** (see Figure 2), and the data is given in Table 3. Fair agreement was found for most bond distances and angles. The calculated bond and torsion angles are within 3° of the X-ray

structures of (R)-**7**. The Ru–P and Cp–Ru bond lengths are within ± 0.05 Å of the experimental value but larger deviations are observed for the P–O and Ru–L bond lengths that are slightly overestimated by the DFT calculations (obviously, the Ru–L bond length cannot be compared with the X-ray structure (L = I), but Ru–I is expected to be larger than Ru–O). Nevertheless the DFT-geometries should give a reasonable picture of the system under investigation here.

The calculated energy barriers for the *I_d* and *D* mechanisms are displayed in Table 4 and shown in Figures 9 and 10.

Gas-Phase Calculations. *D* Mechanism. In the *D* pathway (Figure 6), departure of a water molecule in **A** first leads to the chiral 16-electron species **C**. Inversion of the pyramidal geometry of **C** may then occur via a pendulum movement of the bidentate ligand, through the planar-at-the-metal compound **D**. Alternatively, this movement can also be described as a rocking motion of the Cp ligand with respect to the Ru–P–P plane.

In the theoretical study of the *D* mechanism (singlet electronic pathway), two transition states have been located (see Tables 4 and 5 and Figure 9). The first transition state results from the dissociation of the water molecule (**B**) and is characterized by an imaginary vibrational mode involving almost exclusively the Ru(II)–OH₂ bond (see Table 5). The second transition state (**D**) arises from the rocking motion of the Cp ligand as depicted in Table 5 and has a pseudo-*C*₂-symmetry (φ (Cp–Ru–P–P) = 179.0°).⁴⁹ Furthermore, the lengthening of the Ru–P bonds in **D** (see Table 3) compared with the pyramidal structures **A** and **C** is consistent with the enhanced back-bonding upon pyramidalization.^{15a} In the gas-phase, when neglecting the

(46) Ochterski, J. W. *Thermochemistry in Gaussian*; Gaussian, Inc.: Pittsburgh, PA, 2002.

(47) McQuarrie, D. A. *Statistical Thermodynamics*; Harper and Row: New York, 1973.

(48) Senn, H. M.; Margl, P. M.; Schmid, R.; Ziegler, T.; Blöchl, P. E. *J. Chem. Phys.* **2003**, *118*, 1089.

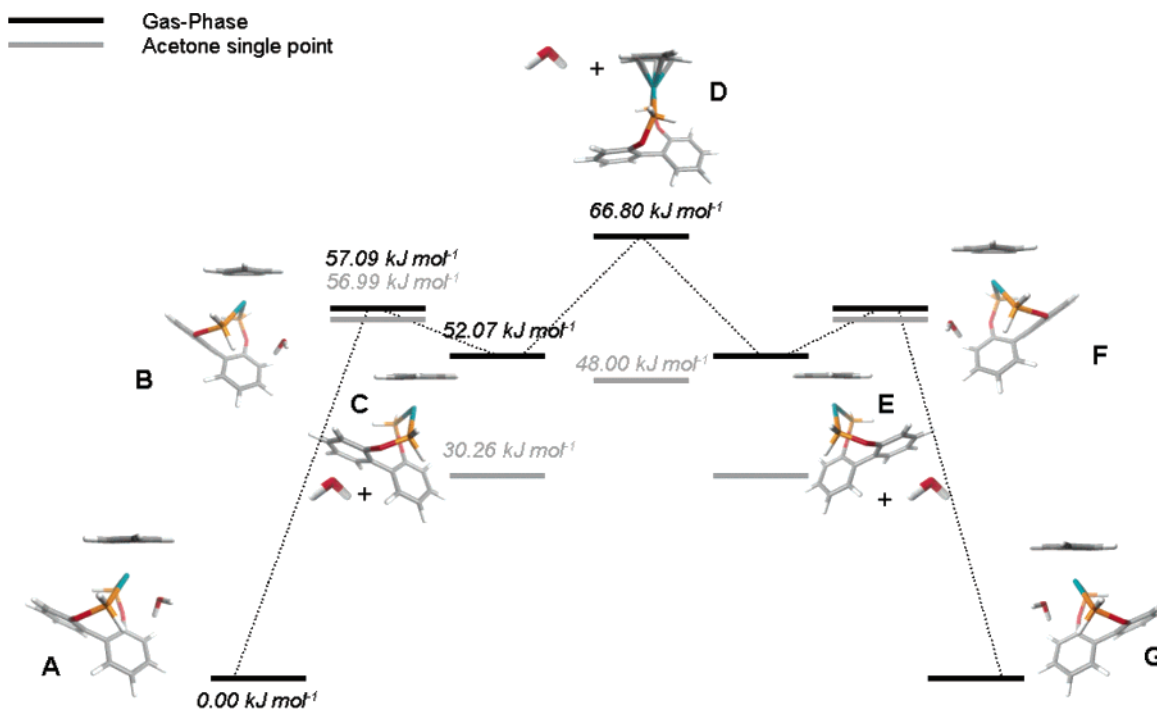


Figure 9. Free energy scheme of the dissociative mechanism.

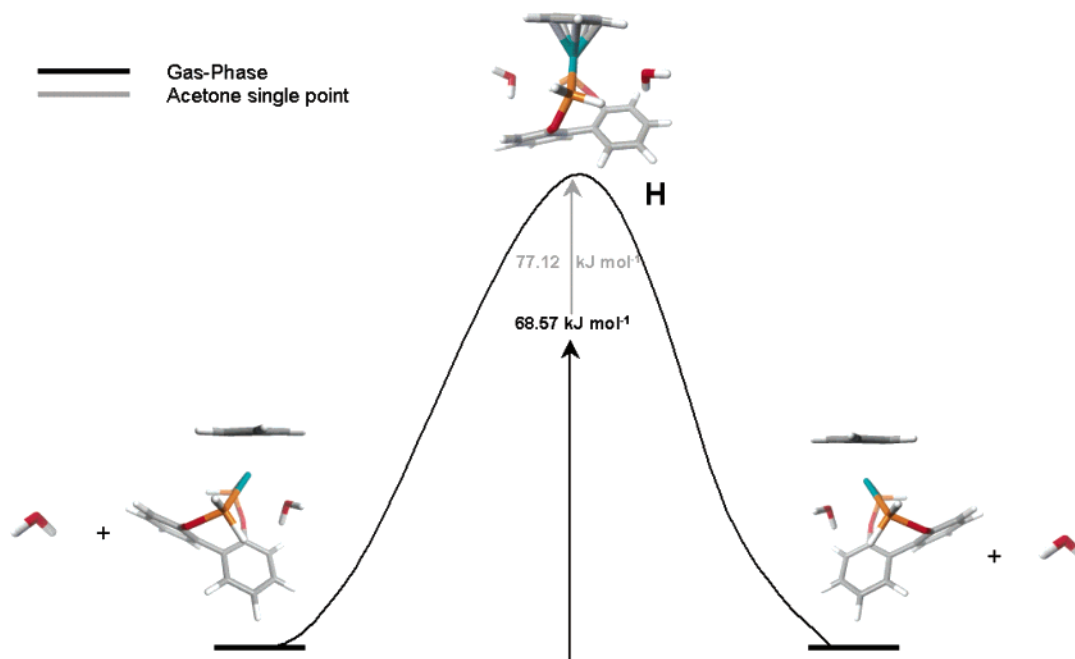


Figure 10. Free energy scheme of the I_d mechanism.

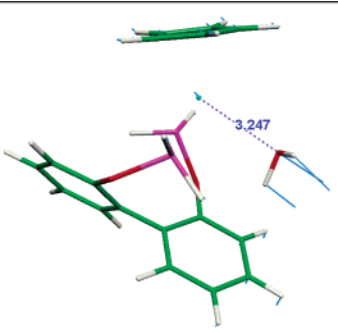
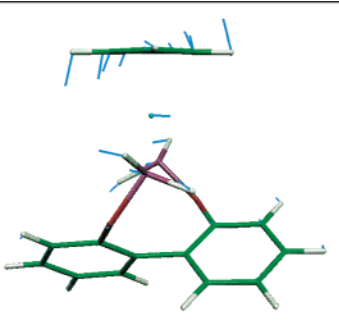
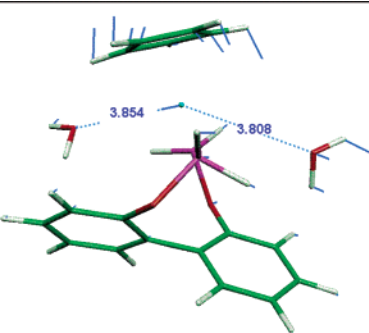
thermal and entropic contributions, the intermediate **C** is at a higher energy than the transition state **B** (see Table 4). Stabilization of **C** is thus strongly linked to the larger translational entropy resulting from the increase in the number of particles (one reactant, two products), as is characteristic for dissociative reactions (see terms T^*S_{trans} for **A**, **C**, and H_2O in Table S-11, 13, and 16 in Supporting Information).

(49) Triplet **D** has also been investigated. The energy required to change the spin state cannot be directly evaluated since it is required that both states possess similar geometries and energies for the spin crossing to occur. In this study, the relative energy of **C** and **D** as triplet species was used to estimate the inversion barrier. This turns out to be considerably larger than in the singlet electronic pathway (63.1 vs 14.6 kJ mol^{-1} for E_{ele}).

Comparison to literature data⁴² of an analogous interconversion for the complex $[(\eta^6\text{-C}_6\text{H}_6)\text{Ru}(\text{C}_6\text{H}_4\text{-2-CH}_2\text{NMe}_2)(\text{NCMe})]^+\text{PF}_6^-$ is of interest. The dissociation of the ligand was not investigated in that case, but approximations were similar to ones we have made (truncated species, solvent and counterion neglected). The relative energy between the minima corresponding to (**A**) and intermediate (**C**) as well as between their intermediate (**C**) and transition state (**D**) are, respectively, within 6.3 and 3.9 kJ mol^{-1} of our gas-phase values.

I_d Mechanism. In case of the I_d mechanism, a single transition state (**H**, Figure 10) has been located. The imaginary

Table 5. Imaginary Mode of the Calculated Transition States

		
B -98.01 cm ⁻¹	D -113.74 cm ⁻¹	H -101.38 cm ⁻¹

mode involves a concerted motion of the leaving water molecule with the rocking motion of the Cp ligand (see Table 5). The transition state was found to deviate from the expected pseudo-*C*₂-symmetry (see Table 3, $\varphi(\text{Cp}_{\text{centroid}}-\text{Ru}-\text{P}-\text{P}) = -175.0^\circ$ and $\Delta(\text{Ru}-\text{O}) = 0.04 \text{ \AA}$). The latter, which has also been located (5 kJ higher in energy), has two coupled imaginary frequencies and hence is a hyper saddle point having no relevance. As shown in Tables 3 and 5, the bond lengths of the incoming and leaving water ligands are 3.81 and 3.85 Å, respectively. The Ru–O bond of the leaving water molecule is elongated by 1.6 Å compared to the equilibrium structure, indicative of the dissociative nature of the interchange. When considering the electronic term only, the energy barrier is lower than that found for the *D* mechanism (+52.07 kJ mol⁻¹). However, for the reasons already mentioned previously, translational entropy disfavors the transition state **H** and actually lies 11.48 kJ mol⁻¹ higher in energy than **B** and 1.77 kJ mol⁻¹ higher than **D**.

Effect of Solvent. So far, the $\Delta G(298.15 \text{ K})$ values have been discussed for the gas-phase (ΔG_{gas}) and not the “liquid”-phase electronic density. As mentioned before, the effects of the solvent (acetone) have been investigated here using a continuum model, and the calculation of Gibbs free energies of reaction in solution (ΔG_{soln}) has been estimated according to eq 3^{50–52}

$$\Delta G^{\text{sol}} = \Delta G^{\text{gas}} + \Delta \Delta G_{\text{soln}} + RT \ln(1/22.4) \quad (3)$$

where $\Delta \Delta G_{\text{soln}}$ is the difference in free energy of solvation between the different structures (ΔG_{soln}) computed using PCM techniques.⁴⁵ Note that a correction term^{51,53} ($RT \ln(1/22.4) = -7.71 \text{ kJ mol}^{-1}$) is necessary to account for the change of reference state from gas phase (ideal gas) to solution. Of course, continuum models are by nature unable to account explicitly for specific solute–solvent interactions, but they have been quite successful in describing the general aspects of solvation.⁴⁴ In the calculations reported here, gas-phase geometries were used for the PCM calculations because structure optimization (carried out for some structures; see Tables S-11 and S-13 in Supporting

Information) indicated only very small changes ($<2 \text{ kJ mol}^{-1}$, $<0.5 \text{ \AA}$, $<1^\circ$).

As shown in Table 4, the largest values of $\Delta \Delta G_{\text{soln}}$ are observed between **A** and **C** (14.10 kJ mol⁻¹) and **A** and **D** (11.09 kJ mol⁻¹). Its origin lies in the solvation energy of the separated molecules and the complex. The separation of one charged molecule (**A**) into another charged molecule (**C**) and a water molecule is strongly favored in polar solvent because of the latter’s dipole moment. As a consequence, when solvent effects are included, the free energy of both **C** and **D** is lowered, while the energy of **B** remains fairly unchanged. For similar reasons, the energy of transition state **H** increases (+16.26 kJ mol⁻¹). The effect of an acetone environment thus distinctly favors the *D* mechanism over the *I_d* mechanism.

It is clear that because of the approximations made,⁵⁵ the computed values cannot be directly correlated with the experimental value $\Delta G^{\ddagger 298}$ displayed in Table 1 (+50.65 ± 0.40 kJ mol⁻¹), but it is likely, nevertheless, that a *D* mechanism is energetically favored at 298 K.

Concluding Remarks

The combined NMR and theoretical studies support a dissociative mechanism for the inversion of the ruthenium center geometry of [Cp((*R*)-BINOP-F)(H₂O)][SbF₆] (*R*)-**8** in acetone. Previous theoretical studies^{15a} on half-sandwich complexes [CpML¹L²L³] gave inversion barriers lower than 15 kcal mol⁻¹. The data on complex (*R*)-**8** do not challenge this finding, but it must be emphasized that the theoretical estimate of free energy values should be taken with caution. Provided that the mechanism that leads to this “inversion” at the chirotopic metal center does not involve partial dissociation of the chiral ligand, it is not expected to lead to an erosion of product enantioselectivity in catalysis. An identical stereochemical environment exists in the catalyst–substrate complex at all times. Conversely, in analogous enantiomerically pure complexes devoid of ligand-based chirality, this inversion leads to racemization at the metal. While the prospect of using “chiral at the metal” complexes as catalysts is a very attractive proposition, this may only be

(50) Aquino, A. J. A.; Tunega, D.; Haberhauer, G.; Gerzabek, M. H.; Lischka, H. *J. Phys. Chem. A* **2002**, *106*, 1862.

(51) Tunega, D.; Haberhauer, G.; Gerzabek, M.; Lischka, H. *J. Phys. Chem. A* **2000**, *104*, 6824.

(52) Colominas, C.; Teixido, J.; Cemeli, J.; Luque, F. J.; Orozco, M. *J. Phys. Chem. B* **1998**, *102*, 2269.

(53) Cieplak, P.; Kollman, P. A. *J. Am. Chem. Soc.* **1988**, *110*, 3734.

(54) Ayala, P. Y.; Schlegel, H. B. *J. Chem. Phys.* **1998**, *108*, 2315.

(55) Structure truncation apart, entropy contributions are based on the assumption that the contributions to the binding in the gas phase and in solution is the same. Stranks, D. R. *Pure Appl. Chem.* **1974**, *38*, 303.

realizable with complexes that link the auxiliary arene or Cp ligand with the other ligands and hence suppress racemization.^{6f}

Experimental Section

General Methods. All synthetic manipulations were carried out using standard Schlenk techniques under an inert atmosphere. All solvents were dried and distilled before use according to standard laboratory procedures. ¹H, ³¹P, and ¹³C NMR spectra were recorded on Bruker AMX400 and Bruker Avance 500 spectrometers. Iodoform and AgSbF₆ were purchased from Fluka. Ru₃(CO)₁₂ was prepared according to the literature.²⁰ The Diels–Alder reaction of methacrolein with cyclopentadiene catalyzed by (*R*)-**7** and (*R*)-**8** was realized following previously described procedures.²

All ³¹P and ¹⁷O NMR spectra for the determination of the kinetic parameters were recorded on a Bruker ARX400 spectrometer operating at 162 and 54 MHz, respectively. The temperature was determined by substituting the sample with a Pt-100 resistor.⁵⁶ The variable-pressure measurements to determine the activation volumes were performed between 0.1 and 200 MPa using a homemade high-pressure NMR probe.⁵⁷ The observed rate constants were obtained by NMR line-shape analysis using the program NMRICMA.⁵⁸ The analyses of the rate constants using the required equations were accomplished with a nonlinear least-squares fitting program. All experimental data are given in Supporting Information. The reported errors represent standard deviations.

(*R*)-BINOP-F (*R*)-4. A solution of (C₆F₅)₂PBr (10.01 g, 22.50 mmol) in anhydrous Et₂O (6 mL) at room temperature was added dropwise to a solution of (*R*)-BINOL (3.22 g, 11.25 mmol) and Et₃N (3.14 mL, 22.53 mmol) in anhydrous Et₂O (100 mL) at 10 °C under an N₂ atmosphere. The resulting white suspension was stirred at 10 °C for 2 h and then at room temperature for 16 h. The mixture was filtered over Celite under N₂, and the Celite was rinsed with Et₂O. The solvent was then evaporated, and the white residue was further purified by recrystallization from hexane (60 mL) to give (*R*)-BINOP-F as a white solid (8.99 g, 79%). ¹H NMR (500 MHz, CD₂Cl₂, rt, SiMe₄): δ = 7.92 (d, *J* = 9.2 Hz, 2H), 7.81 (d, *J* = 8.2 Hz, 2H), 7.48 (d, *J* = 8.8 Hz, 2H), 7.41 (ddd, *J* = 8.2, 6.9, 1.3 Hz, 2H), 7.25 (ddd, *J* = 8.2, 7.0, 1.3 Hz, 2H), 7.00 (d, *J* = 8.5 Hz, 2H). ¹³C NMR (125 MHz, CD₂Cl₂, rt, SiMe₄): δ = 152.7 (d, *J*(C,P) = 16.1 Hz), 133.6, 131.0, 128.1, 127.5, 125.8, 125.7, 122.5 (d, *J*(C,P) = 9.2 Hz), 119.9 (d, *J*(C,P) = 9.2 Hz). ¹⁹F NMR (470 MHz, CD₂Cl₂, rt, C₆F₆): δ = 31.17–30.95 (m, 4F), 30.59–30.38 (m, 4F), 14.15 (tm, *J* = 19.8 Hz, 2F), 13.20 (tm, *J* = 19.9 Hz, 2F), 2.81–2.63 (m, 4F), 2.34–2.17 (m, 4F). ³¹P NMR (202 MHz, CD₂Cl₂, rt, H₃PO₄): δ = 89.0 (qm, *J*(P,F) = 32 Hz). [α]_D (20 °C, *c* 0.95, hexane): +88.7

[CpRu(*R*)-BINOP-F]H (*R*)-5. Cyclopentadiene (4.40 mL, 53.60 mmol) was added to an orange solution of Ru₃(CO)₁₂ (426 mg, 0.67 mmol) in refluxing anhydrous heptane (120 mL), and the mixture was heated at reflux for 2 h under an N₂ atmosphere. The resulting yellow solution was then cooled to 80 °C; (*R*)-BINOP-F (*R*)-**4** was added, and the mixture was refluxed for 17 h. The solution was cooled to room temperature, and the solvent was evaporated; the yellow residue was purified by chromatography (aluminum oxide, neutral) with hexane and then toluene. The yellow band was collected, and the volatiles were removed in vacuo, yielding the hydrido complex (*R*)-**5** (2.06 g, 81%) as a yellow solid. ¹H NMR (CD₂Cl₂, 500 MHz, rt): δ 7.87 (d, *J* = 9.1 Hz, 1H), 7.79 (d, *J* = 9.1 Hz, 1H), 7.77 (d, *J* = 9.1 Hz, 1H), 7.67–7.61 (m, 3H), 7.38–7.31 (m, 2H), 7.20–7.16 (m, 1H), 7.15–7.10 (m, 1H), 6.81 (d, *J* = 8.5 Hz, 1H), 6.63 (d, *J* = 8.5 Hz, 1H), 4.39 (s, 5H), –11.82 (ddd, *J*(H,P) = 41.2, 38.2 Hz, *J*(H,F) = 3 Hz, 1H). ¹³C NMR (CD₂Cl₂, 125 MHz, rt): δ 152.2 (d, *J*(C,P) = 2.3 Hz), 150.0 (d, *J*(C,P)

= 2.3 Hz), 133.4, 133.2, 131.3, 131.0, 130.7, 130.6, 127.9, 127.6, 127.5, 127.4, 126.2, 126.0, 125.3, 124.9, 124.3 (d, *J*(C,P) = 3.4 Hz), 123.4–123.2 (m), 123.0–122.9 (m), 86.5. ³¹P NMR (CD₂Cl₂, 202 MHz, rt): δ 115.6 (q_{AB}, Δ*v*_{AB} = 2404 Hz, *J*_{AB} = 50 Hz).

[CpRu(*R*)-BINOP-F] (*R*)-6. A yellow suspension of (*R*)-**5** (1.48 g, 1.25 mmol) and iodoform (4.92 g, 12.50 mmol) in acetone (12.50 mL) was refluxed for 28 h. The solution was cooled to room temperature, and the solvent was evaporated; the orange residue was purified by chromatography (silica) with a mixture of pentane and CH₂Cl₂ (10:1 to 1:1). The orange band was collected, and the volatiles were removed in vacuo. The orange residue was then recrystallized from CH₂Cl₂/MeOH to give the iodo complex (*R*)-**6** (1.19 g, 72%) as orange crystals. ¹H NMR (CD₂Cl₂, 500 MHz, rt): δ 8.09 (d, *J* = 9.1 Hz, 1H), 7.85 (d, *J* = 9.1 Hz, 1H), 7.81 (d, *J* = 9.1 Hz, 1H), 7.70 (d, *J* = 7.9 Hz, 1H), 7.67 (d, *J* = 8.2 Hz, 1H), 7.45 (d, *J* = 9.1 Hz, 1H), 7.37 (ddd, *J* = 7.9, 6.6, 1.3 Hz, 1H), 7.34 (ddd, *J* = 8.2, 7.0, 1.3 Hz, 1H; C₁₀H₁₂), 7.15 (ddd, *J* = 8.2, 6.6, 1.3 Hz, 1H), 7.08 (ddd, *J* = 8.2, 7.0, 1.3 Hz, 1H), 6.63 (d, *J* = 8.5 Hz, 1H), 6.45 (d, *J* = 8.5 Hz, 1H), 4.72 (s, 5H). ¹³C NMR (CD₂Cl₂, 125 MHz, rt): δ 150.9 (d, *J*(C,P) = 4.0 Hz), 149.3 (d, *J*(C,P) = 4.0 Hz), 133.7, 133.4, 131.3, 131.2, 130.7, 130.4, 128.0, 127.9, 127.7, 127.2, 126.5, 126.1, 125.4, 125.2, 125.0, 122.6 (d, *J*(C,P) = 3.4 Hz), 122.5 (d, *J*(C,P) = 2.3 Hz), 122.1, 88.1. ³¹P NMR (CD₂Cl₂, 202 MHz, rt): δ 113.8 (q_{AB}, Δ*v*_{AB} = 1258 Hz, *J*_{AB} = 66 Hz).

[CpRu(*R*)-BINOP-F(Acetone)][SbF₆] (*R*)-7. A solution of AgSbF₆ (952 mg, 2.71 mmol) in dried CH₂Cl₂ (27 mL) was added at room temperature to (*R*)-**6** (784 mg, 0.60 mmol) in a mixture of dried acetone (10 mL) and CH₂Cl₂ (13 mL). The mixture was stirred at room temperature for 30 min. After evaporation of the solvent under vacuum, the residue was dissolved in a 1:1 mixture of acetone and CH₂Cl₂ and filtered through Celite. After evaporation of volatiles under vacuum, the product was purified by dissolution in acetone and precipitation by addition of Et₂O to give compound (*R*)-**7** as an orange solid (847 mg, 95%). ¹H NMR (acetone-*d*₆, 400 MHz, 40 °C): δ 8.13 (d, *J* = 9.1 Hz, 2H), 7.87 (d, *J* = 8.1 Hz, 2H), 7.73 (d, *J* = 9.1 Hz, 2H), 7.47 (dd, *J*₁ = 8.1 Hz, *J*₂ = 7.3 Hz, 2H), 7.26 (dd, *J*₁ = 8.1 Hz, *J*₂ = 7.3 Hz, 2H), 6.58 (d, *J* = 8.1 Hz, 2H), 5.07 (s, 5H). ¹H NMR (acetone-*d*₆, 400 MHz, –40 °C): δ 8.18 (d, *J* = 9.6 Hz, 2H), 8.00–7.94 (m, 2H), 7.77–7.70 (m, 2H), 7.54–7.46 (m, 2H), 7.35–7.23 (m, 2H), 6.57 (d, *J* = 8.6 Hz, 1H), 6.42 (d, *J* = 8.3 Hz, 1H), 5.14 (s, 5H). ¹³C NMR (acetone-*d*₆, 100 MHz, 40 °C): δ 150.8, 133.8, 133.0, 131.9, 128.8, 128.8, 127.4, 125.5, 123.0, 122.2, 87.2. ³¹P NMR (acetone-*d*₆, 162 MHz, 40 °C): δ 123.8. ³¹P NMR (acetone-*d*₆, 162 MHz, –40 °C): δ 124.3 (q_{AB}, Δ*v*_{AB} = 2931 Hz, *J*_{AB} = 64 Hz).

[CpRu(*R*)-BINOP-F(H₂O)][SbF₆] (*R*)-8. H₂O (9 μL, 0.5 mmol) was added to an orange solution of (*R*)-**7** (125 mg, 0.085 mmol) in CH₂Cl₂ (1 mL) at room temperature. The solution was stirred for 5 min, and the volatiles were removed in vacuo. The solid residue was dissolved in CH₂Cl₂ (1 mL); water (9 μL, 0.5 mmol) was added, and the solution was stirred for 5 min before the volatiles were evaporated under vacuum. Another cycle of dissolution–addition of water–stirring–evaporation gave the aquo complex (*R*)-**8** as a yellow solid (120 mg, 98%). ¹H NMR (acetone-*d*₆, 400 MHz, 25 °C): δ 8.10 (d, *J* = 9.1 Hz, 2H), 7.86 (d, *J* = 8.1 Hz, 2H), 7.73 (d, *J* = 9.1 Hz, 2H), 7.47 (dd, *J*₁ = 8.1 Hz, *J*₂ = 7.2 Hz, 2H), 7.26 (dd, *J*₁ = 8.1 Hz, *J*₂ = 7.2 Hz, 2H), 6.60 (d, *J* = 8.1 Hz, 2H), 5.04 (s, 5H). ¹H NMR (acetone-*d*₆, 400 MHz, –40 °C): δ 8.16 (d, *J* = 9.1 Hz, 2H), 7.94–7.90 (m, 2H), 7.73–7.69 (m, 2H), 7.51–7.45 (m, 2H), 7.30–7.22 (m, 2H), 6.61 (d, *J* = 8.6 Hz, 1H), 6.45 (d, *J* = 8.6 Hz, 1H), 5.71 (bs, 2H), 5.06 (s, 5H). ¹³C NMR (acetone-*d*₆, 100 MHz, 40 °C): δ 149.8, 132.9, 131.8, 130.8, 127.7, 126.4, 124.5, 121.8, 121.6, 86.0. ¹³C NMR (100 MHz, acetone-*d*₆, –40 °C): δ 149.8, 148.1, 132.0, 131.4, 131.0, 130.8, 130.2, 129.6, 127.3, 127.0, 126.9, 125.7, 125.5, 123.7, 123.4, 121.6, 121.3, 119.7, 86.5. ³¹P NMR (acetone-*d*₆, 162 MHz, 25 °C): δ 123.3. ³¹P NMR (acetone-*d*₆, 162 MHz, –40 °C): δ 122.9 (q_{AB}, Δ*v*_{AB} = 2439 Hz, *J*_{AB} = 61 Hz).

(56) Amann, C.; Meyer, P.; Merbach, A. E. *J. Magn. Reson.* **1982**, *46*, 319.

(57) Cusanelli, A.; Nicula-Dadaci, L.; Frey, U.; Merbach, A. E. *Inorg. Chem.* **1997**, *36*, 2211.

(58) Helm, L.; Borel, A.; NMRICMA; Lausanne University: Lausanne, Switzerland, 1998.

X-ray Crystallographic Analysis. Cell dimensions and intensities were measured at 200 K on a Stoe STADI4 diffractometer with graphite-monochromated Cu K α radiation ($\lambda = 1.5418 \text{ \AA}$) for [CpRu((R)-BINOP-F)] (*R*)-**6** and on a Stoe IPDS diffractometer with graphite-monochromated Mo K α radiation ($\lambda = 0.71073 \text{ \AA}$) for [CpRu((R)-BINOP-F)(acetone)][SbF₆] (*R*)-**7**. Data were corrected for Lorentz and polarization effects and for absorption. The structures were solved by direct methods (SIR97),⁵⁹ and all other calculations were performed with XTAL system⁶⁰ and ORTEP⁶¹ programs. [CpRu((R)-BINOP-F)] (*R*)-**6**: C₅₀H₁₉Cl₂F₂₀IO₂P₂Ru, $M = 1392.5$, $d_x = 1.901 \text{ g cm}^{-3}$, orthorhombic, $P2_12_12_1$, $Z = 4$, $a = 13.038(1)$, $b = 16.812(1)$, $c = 22.199(2) \text{ \AA}$, $U = 4865.9(2) \text{ \AA}^3$; 6880 measured reflections, 5979 unique reflections of which 5272 were observables ($|Fo| > 4\sigma(Fo)$). Full-matrix least-squares refinement based on F gave final values $R = 0.043$, $\omega R = 0.042$, and Flack parameter $x = 0.00(1)$. Hydrogen atoms of the complex were placed in calculated positions. [CpRu((R)-BINOP-F-

(acetone)][SbF₆]. [Et₂O] (*R*)-**7**: C₅₆H₃₃F₂₆O₄P₂RuSb; $M = 1548.6$, $d_x = 1.643 \text{ g cm}^{-3}$, orthorhombic, $P2_12_12_1$, $Z = 4$, $a = 13.4024(7)$, $b = 19.3137(10)$, $c = 24.1839(15) \text{ \AA}$, $U = 6260.0(7) \text{ \AA}^3$; 78 798 measured reflections, 12 186 unique reflections of which 7103 were observables ($|Fo| > 4\sigma(Fo)$). Full-matrix least-squares refinement based on F gave final values $R = 0.042$, $\omega R = 0.047$, and Flack parameter $x = -0.01(3)$. Hydrogen atoms of the complex were placed in calculated positions. Both Et₂O solvent molecules are disordered and refined with population parameters of 0.5 and restraints on bond lengths and bond angles.

Acknowledgment. Financial support for this work by the Swiss National Science Foundation is gratefully acknowledged. We thank the Ministère des Affaires Étrangères of France for a Lavoisier grant to V.A.

Supporting Information Available: Listing of experimental data obtained from variable-temperature, -pressure, and -concentration ¹⁷O and ³¹P NMR experiments and X-ray crystallographic files (CIF) for (*R*)-**6** and (*R*)-**7**. This material is available free of charge via the Internet at <http://pubs.acs.org>.

JA0374123

- (59) Altomare, A.; Burla, M. C.; Camalli, M.; Cascarano, G.; Giacovazzo, C.; Guagliardi, A.; Moliterni, A. G. G.; Polidori, G.; Spagna, R. *J. Appl. Cryst.* **1999**, *32*, 115.
(60) Hall, S. R., Flack, H. D., Stewart, J. M., Eds. *XTAL3.2 User's Manual*; Universities of Western Australia and Maryland, 1992.
(61) Johnson, C. K. *ORTEP II*; Oakridge National Laboratory: Oak Ridge, TN, 1976; Report ORNL-5138.